ACS OMEGA

Open Access

http://pubs.acs.org/journal/acsodf

Article

Anionic Dye Removal with a Thin Cationic Polyaniline Coating on Cellulosic Biomaterial

Karima Ferchichi, Amaini Chouchaine, Noureddine Amdouni, Yves Chevalier, and Souhaira Hbaieb*

Cite This: *ACS Omega* 2024, 9, 15935−15949

Read Online

ACCESS | Metrics & More | Article Recommendations

ABSTRACT: This paper reports the development of novel adsorbent materials using polyaniline (PANI) grafted onto Posidonia (POS) fibers, aimed at efficiently removing phenol red (PSP), an anionic dye, from aqueous solutions. The synthesis involved the copolymerization of aniline grafted on the surface of the POS and aniline monomer in solution, resulting in a chemically bound thin PANI layer on the POS bioadsorbent. Structural characteristics and binding affinities of these adsorbents with PANI under its emeraldine salt (POS@PANI-ES) or emeraldine base (POS@PANI-EB) forms are reported. The rapid adsorption kinetics observed are attributed to enhanced accessibility to PANI adsorption sites on the POS surface. The binding percentages of PSP to POS@PANI-ES and POS@PANI-EB materials were found to be 97 and 50%, respectively, after 15 min of contact time. The Langmuir model for localized adsorption sites and the Volmer model for nonlocalized adsorption as a mobile layer were fitted to the experimental adsorption isotherms of PSP to POS@PANI-EB and POS@PANI-ES, yielding the thermodynamic parameters of adsorption. The adsorption capacities of PSP on POS@PANI-EB and POS@PANI-ES were 37.8 and 71.5 μmol g^{-1}, respectively. The adsorption of PSP remained above 80% at moderate salt concentrations of around 0.1 mol L^{-1}; however, higher concentrations of NaCl and $CaCl_2$ in PSP solutions significantly reduced the adsorption on POS@PANI-ES.

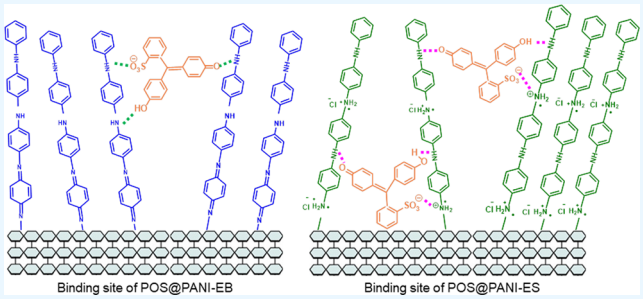

1. INTRODUCTION

Industrial wastewater laden with residual dyes comes from different sources (e.g., dyeing or textile industries, pharmaceutical industries, etc.) and is considered a wide variety of organic pollutants, highly visible even at vanishing concentrations.[1] Their direct release into the environment can lead to the accumulation of toxic substances resulting from the chemical or biochemical transformation of the dyes and the deterioration of the aquatic environment.[2] Often, chemicals in industrial wastewater are difficult to biodegrade, and the inadequacy of treatments leads to their accumulation in the water cycle.[3−5] Dye-laden industrial wastewater has been extensively studied by developing effective dye removal techniques to treat the dye effluents before discharging them into water bodies.[6−10] Conventional physicochemical and biological methods of effluent treatment are expensive and sometimes unsuitable for large rivers due to their less cost-effective and difficult operational conditions. For the removal of organic dyes from aqueous media, many methods have been investigated. The most widely used techniques for water discoloration include adsorption, photodegradation, precipitation, coagulation, and membrane filtration.[11] The most powerful and practical discoloration treatment process among the available water treatment techniques is adsorption, in which recovery and recycling of adsorbent materials can be possible with cost-effectiveness and distinct advantages such as no release of toxic sludge. Nowadays, many inexpensive and commercially available adsorbents have been tried for water discoloration processes such as clays, zeolites, activated alumina, peat, biomasses, biopolymers, agricultural residues, and industrial byproducts.[12] These adsorbents are able to adsorb many dyes contained in industrial aqueous effluents with high adsorption capacities, but the costs of regeneration are high because desorption of the dye molecules is not easy to achieve.[13] In recent years, low-cost adsorbents including products of natural waste origin, such as fruit trees, egg shells, palm waste, and date palm kernels have also been used.[14] However, there is still a need to study new biomaterials with low cost and high adsorption capacities. The objective of this study was to introduce modified Posidonia as an adsorbent for the removal of anionic dyes, such as phenol red, considered a

Received: November 13, 2023
Revised: March 14, 2024
Accepted: March 19, 2024
Published: March 28, 2024

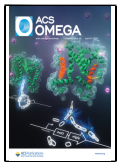

typical dye, from water by adsorption using depletion techniques.

Posidonia oceanica (POS), commonly known as Neptune grass or Mediterranean tapeweed, is an abundant biomass source suitable for producing high-value-added materials. Its ability as an adsorbent to remove both organic and inorganic molecules has been shown.[15−18] The main constituents of fibrous POS materials are cellulose, lignin, and hemicellulose. Its surface is rich in hydroxyl groups, which can be exploited for surface modification. It also contains other functional groups, such as carboxylic acid and amide, that can play an important role in the adsorption process. For example, carboxylic acid groups can contribute to the adsorption of positively charged species through ion exchange and electrostatic interactions. At the same time, amide groups may be involved in hydrogen bonding or other interactions that affect the overall adsorption capacity and mechanism.

Phenol red or phenolsulfonphthalein (PSP), classified as an anionic dye, is a red crystal stable in air and highly soluble in water (0.77 g L^{-1}).[19] The molar mass (M_W) of phenol red is 354.38 g mol^{-1}. It is a pH indicator that changes color from yellow below pH 6.8 to bright pink above pH 8.2. It is commonly used as an indicator in cell culture and various laboratory applications. It is widely used in various industrial processes and even in household products. One application that causes its release in the environment is the control of the pH and chlorination degree in swimming pools.[20] The discharge of phenol red into wastewater raises significant environmental concerns related to its bioaccumulation in aquatic fauna. In addition, phenol red in wastewater can contribute to unpleasant odors and contaminate organic and inorganic substances, thereby exacerbating pollution and environmental problems in the long term. The toxicity of phenol red to microorganisms and aquatic ecosystems highlights the importance of its effective removal from wastewater. Posidonia has a negative surface charge throughout the pH range; it requires surface modification by a cationic polymer. Polyaniline polymer (PANI) was used in the present work because of its favorable chemical structure for electrostatic interactions with PSP. In addition, our previous work[21] has shown that the grafting process by copolymerization of aniline and surface-grafted aniline yields a very thin layer of grafted PANI with an average polymerization degree of approximately 4. A thin grafted layer is enough with regard to the application to adsorption because adsorption takes place on the surface. Using a small amount of grafted material is economically favorable.

To obtain a solid support with suitable functions for the covalent immobilization of the PANI polymer, the preparation involved grafting aniline groups onto the surface of Posidonia. These monomer reactive groups served as precursors for the development of a thin, rigid layer of polyaniline on the surface through their copolymerization with free aniline added in solution. Indeed, PANI in its emeraldine salt form (PANI-ES) is a cationic conjugated polymer produced by the conventional oxidative polycondensation of aniline monomer in an acidic medium. Undoubtedly, the delocalization of charges on the polymer backbone makes PANI a hydrophobic polymer despite its overall polycationic nature. This cationic and hydrophobic structure of PANI-ES allows hydrophobic interactions to be assisted by electrostatic interactions with aromatic and anionic PSP molecules. Indeed, in addition to electrostatic interactions, conjugated aniline moieties create favorable $\pi-\pi$ stacking interactions with polyaromatic molecules, as for example organic dyes.[21] PANI-ES is prepared by oxidative polymerization of aniline in a concentrated aqueous medium of hydrochloric acid (1 M HCl). PANI-ES requires doping of the conjugated polymer by protonation of nitrogen atoms with an acid. Several examples of adsorbent materials prepared from PANI doped in its acidic form have been reported. A more sophisticated preparation of PANI grafted onto the surface of mesoporous silica revealed a selective adsorption capacity for organic sunscreens.[22] As simpler is better, the present work dealt with the polymerization of aniline aiming at the formation of a thin layer of PANI coating the POS bioadsorbent by copolymerization with the surface-grafted aniline (POS@ANI). POS@PANI-EB was prepared by dedoping POS@PANI-ES in a basic medium. The produced materials were evaluated and compared by means of adsorption tests involving the kinetics of the adsorption process and adsorption equilibrium isotherms. This study presents a novel adsorbent material with promising applications in the removal of anionic dyes from wastewater. By exploiting the unique properties of the PANI-coated POS, this research contributes to the development of sustainable and cost-effective solutions for wastewater treatment.

2. MATERIALS AND METHODS

2.1. Reagents and Chemicals. Aniline (ANI), *N*-[3-(trimethoxysilyl)propyl]aniline (APTMS), diisopropylethylamine (DIEA), ammonium persulfate, and phenol red also known as phenolsulfonphthalein (PSP) were supplied by Sigma-Aldrich. All solvents used were of analytical grade, and all solutions were made with Milli-Q water of 18 MΩ·cm resistivity.

2.2. Characterization Methods. Infrared (IR) spectra were recorded with a Bruker IFS 55 Equinox Fourier transform IR (FTIR) spectrometer in the attenuated total reflectance (ATR) mode. ^{13}C cross-polarization magic-angle-spinning (CP-MAS) NMR spectra of native and modified Posidonia materials were performed on a Bruker Avance III 500 ultrashield PLUS spectrometer. All prepared Posidonia materials were subjected to thermogravimetric analyses (TGA) carried out on a TG209F1 Netzsch instrument under a dynamic atmosphere of nitrogen. ζ-Potentials were measured by electrophoresis with a Malvern Zetasizer Nano ZS instrument, with 0.05 wt % aqueous suspensions at different pH values. The ζ-potential was calculated from the electrophoretic mobility under the Smoluchowski approximation. The measurements were carried out using the suspensions of materials in ultrapure water and adjusting the pH of each (values between 2 and 10) by the addition of 0.1 M NaOH or HCl solution. The suspensions were kept under constant agitation at ambient temperature for 24 h to determine the final equilibrium pH. PSP absorbance was measured using an ultraviolet−visible (UV−vis) spectrophotometer of Varian Cary 50 type. The X-ray diffraction (XRD) profiles were obtained using a PANalytical X'Pert PRO Multi-Purpose diffractometer with Cu Kα radiation at a generator voltage of 45 kV and current of 40 mA. The full nitrogen adsorption−desorption isotherms were performed at 77 K using a Micromeritics ASAP2020 instrument. Before nitrogen adsorption measurements, the MIPs were heated at 150 °C under a vacuum. The Brunauer−Emmett−Teller (BET) method was used to calculate the specific surface area of the MIPs. The porous volumes were calculated from the experimental

https://doi.org/10.1021/acsomega.3c09031
ACS Omega 2024, 9, 15935−15949

desorption branch according to the Barret−Joyner−Halenda (BJH) method. Measurements of nitrogen adsorption−desorption isotherms were performed at 77 K by using a Micromeritics ASAP2020 instrument. Before nitrogen adsorption measurements, the samples were degassed at 150 °C under a vacuum. The specific surface area was calculated by the Brunauer−Emmett−Teller (BET) method. Optical microscopy pictures of aqueous suspensions were taken between plate and coverslip using a Leica DMLM microscope. Scanning electron microscopy (SEM) pictures were taken at the Centre Technologique des Microstructures facility of the University of Lyon 1 (CTmu, https://microscopies.univ-lyon1.fr/) using a FEI Quanta 250 FEG microscope working under 5 kV acceleration and secondary electron detection. Powder samples were spread on aluminum stubs covered with double-sided conductive adhesive carbon disks (Agar, Oxford Instruments) and metalized by sputtering Cu in a Leica MED 020 coating system.

2.3. Preparation of Posidonia Biomaterials. Posidonia balls were collected from the Cheba-Mahdia beach on the east coast of Tunisia. The fibers of biomass balls have been manually disentangled, extensively washed with large volumes of deionized water to remove sand and salt commonly present in seawater, and then dried in the open air. The obtained Posidonia fibers were washed in a Soxhlet extractor with ethanol for 24 h and dried in an oven at 50 °C for 48 h until the mass of the fibers became constant. The dry biomasses were crushed, then sieved in order to recover particles of homogeneous size (50 μm), washed repeatedly with distilled water, and oven-dried for 24 h at 50−60 °C. The Posidonia samples were stored in a desiccator for later use.

2.4. Grafting of Aniline Monomer to Posidonia Surface. The anhydrous process involving a direct reaction of surface silanols was investigated for the grafting of *N*-[3-(trimethoxysilyl)propyl]aniline silane (APTMS) as a dense monolayer at the surface of Posidonia; 500 mg of dried Posidonia (POS) was dispersed by magnetic stirring in 17 mL of anhydrous toluene containing 400 mg of APTMS and 400 mg of DIEA. The suspension was heated at reflux under a nitrogen atmosphere for 12 h. The modified Posidonia (POS@ANI) was rinsed with 30 mL of THF, dried at 60 °C overnight, and stored under a vacuum for subsequent uses.

2.5. Coating-Modified Posidonia with Polyaniline. The aniline monomer grafted to the surface of prepared POS@ANI was copolymerized with aniline; 500 mg of POS@ANI was dispersed in 100 mL of HCl aqueous solution at pH = 3 in the presence of 186 mg (2 mmol) of aniline monomer. The reaction mixture was cooled in an ice bath, and 5 mL of a solution of ammonium persulfate in water was added dropwise to the solution. The reaction was allowed to proceed at 0−5 °C for 8 h. The POS@PANI-ES powder was isolated by filtration and washed repeatedly with water until the characteristic UV absorption of PANI oligomers at 400 and 800 nm was absent in the filtrate. Then, the solid powder was dried under vacuum at 60 °C for 24 h.

The POS@PANI-EB was prepared by treatment of POS@PANI-ES with a 0.3 M NH_4OH solution for 24 h. The list of abbreviations of materials used to carry out this work is reported in Table 1.

Table 1. List of the Studied Materials and Their Abbreviations

materials	abbreviations
posidonia powder (medium size 50 μm)	POS
posidonia modified with aniline	POS@ANI
posidonia modified with PANI-EB	POS@PANI-EB
posidonia modified with PANI-ES	POS@PANI-ES

2.6. Binding Experiments. *2.6.1. Standard Solutions.* Stock standard solutions (300 μmol L^{-1}) of phenol red were prepared in water. Working solutions ranging from 10 to 250 μmol L^{-1} were obtained by successive dilutions in water at neutral pH. Both stock standard and working standard solutions were stored in a refrigerator at 5 °C until their use.

2.6.2. Effect of Adsorbent Mass. The experiments were carried out by agitating 5 mL of 50 μmol L^{-1} PSP solutions with varying amounts of unmodified or modified Posidonia (POS, POS@PANI-ES, and POS@PANI-EB) at 298 K. Subsequent to centrifugation of each sample, the residual PSP concentration was measured by using a UV−vis spectrophotometer at the appropriate wavelength (λ_{max} = 430 nm). The adsorbed percentage (%*A*, %) was calculated using the following equation:

$$\%A = (C_0 - C_e)\frac{100}{C_0} \quad (1)$$

where C_e (mol L^{-1}) is the equilibrium concentration of PSP solution, C_0 is the initial PSP concentration (mol L^{-1}), V (L) is the volume of PSP solution, and m (g) is the mass of the adsorbent.

2.6.3. Kinetic Study. Kinetic studies were established to evaluate the effect of the contact time on PSP adsorption and to determine the equilibrium time. The adsorption process was conducted for the time intervals of 2, 5, 8, 12, 16, 20, 25, 30, 40 and 50 min at 298 K. The initial concentration of PSP aqueous solution was fixed at 50 and 100 μmol L^{-1}. 18 mg of each prepared material was mixed with 5 mL of PSP solution, and the mixture was then magnetically stirred at 380 rpm for different contact times. After each stirring, the mixture was centrifuged at 5000 rpm. The supernatant was analyzed by UV−vis absorbance analysis at λ_{max} = 430 nm. The percentage of adsorbed amount at time t (Q_t, mol g^{-1}) was calculated using the following equation:

$$Q_t = \frac{V}{m}[C_0 - C_t] \quad (2)$$

where C_t (mg L^{-1}) is the residual PSP concentration at time t, C_0 is the initial PSP concentration (mg L^{-1}), V (L) is the volume of PSP solution, and m (g) is the mass of the material.

2.6.4. Adsorption Isotherms. All adsorption measurements were performed by the depletion method in water since real environmental samples were essentially aqueous media. For equilibrium adsorption, the material (18 mg) was immersed in 5 mL of water containing PSP with various concentrations ranging from 10 to 175 μmol L^{-1} and kept in a thermostatic water bath shaker and shaken at 380 rpm constant shaking rate at a constant temperature. The mixture was stirred for 60 min equilibration time and then centrifuged at 5000 rpm The residual PSP concentration (C_e, mol L^{-1}) in the supernatant was determined by UV−vis absorbance analysis (λ_{max} = 430 nm) using the calibration curve. The dynamic adsorption capacity (Q_e, mol g^{-1}) of PSP was calculated according to the following equation:

$$Q_e = \frac{V}{m}(C_0 - C_e) \quad (3)$$

https://doi.org/10.1021/acsomega.3c09031
ACS Omega 2024, 9, 15935−15949

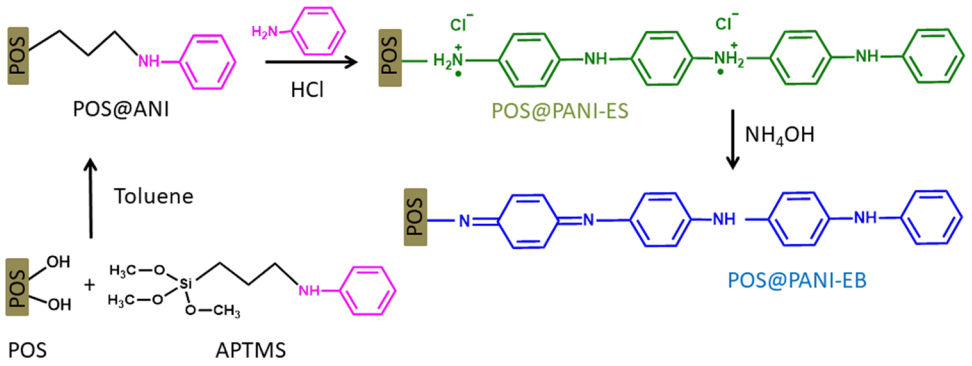

Figure 1. PANI synthesis route in emeraldine salt and emeraldine base forms immobilized on the POS biomaterial.

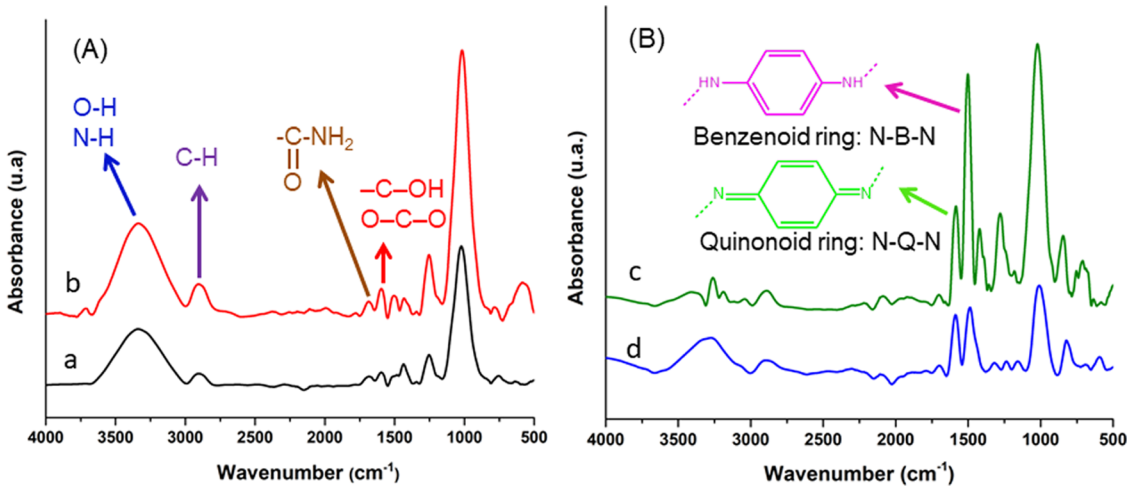

Figure 2. IR spectra of (A) POS (a), and POS@ANI (b) and (B) POS@PANI-ES (c) and POS@PANI-EB (d).

where C_0 (mol L^{-1}) and C_e (mol L^{-1}) are the initial and equilibrium concentrations of the PSP solution, respectively, V (L) is the volume of the PSP solution, and m (g) is the mass of the solid material.

3. RESULTS AND DISCUSSION

3.1. Synthesis and Characterization of Polyaniline Grafted on Posidonia. The Posidonia biomaterial exhibits numerous surface functional groups that serve as readily accessible sites for grafting. These functional groups present on the surface of Posidonia, such as hydroxyl, carboxyl, and amino groups, offer versatile and reactive points for chemical interactions and modifications. This inherent reactivity allows for the seamless incorporation of various functional moieties, including polyaniline in this case, through well-established chemical methods. Indeed, the preparation of POS@PANI-ES and POS@PANI-EB was achieved in two synthetic steps (Figure 1): *N*-[3-(trimethoxysilyl)propyl]aniline (APTMS) containing aniline group was first grafted onto POS surface to provide POS@ANI with anchored aniline monomers available for subsequent copolymerization. The silane coupling agent was covalently attached to the POS surface by a direct condensation reaction of surface functional groups of Posidonia with the methoxy groups of APTMS involving an anhydrous process. Such a process allows binding of a dense monolayer of aniline monomer at the surface of Posidonia. Thus, the aniline groups in APTMS immobilized onto the POS biomaterial have strong reactivity and can effectively be involved in the oxidative polymerization of aniline. The POS@PANI-ES material was prepared by oxidative copolymerization of aniline groups of POS@ANI and aniline monomer added to the acidic reaction medium. The polymerization of aniline was achieved in an acidic medium (HCl concentration in the range 10^{-3} M, pH = 3) for producing the cationic PANI-ES form grafted on the surface of Posidonia. At this pH, aniline is predominantly protonated under anilinium form, and the generated polyaniline is under its emeraldine salt form. A grafted PANI-ES layer was formed on the surface of Posidonia. POS@PANI-EB was prepared by treatment of POS@PANI-ES with a 0.3 M aqueous ammonia solution.

Infrared spectra of POS, POS@ANI, POS@PANI-ES, and POS@PANI-EB were collected in the wavenumber range 500−4000 cm^{-1} (Figure 2A,B). The characteristic bands of the POS biomaterial indicate the presence of carbonyl, hydroxyl, and methoxy functional groups, which are characteristics of cellulose, hemicellulose, and lignin, respectively (Figure 2A). The presence of −OH and − NH vibrations was demonstrated by the broad band in the range 3700−3000 cm^{-1}. The asymmetric and symmetric C−H stretching vibrations located at 2971 and 2886 cm^{-1} are assigned to the alkyl groups, respectively. The band at 1617 cm^{-1} was attributed to the amide $-C(O)NH_2$ bond, while the one at 1425 cm^{-1} was related to the deformation vibration of −C−OH, featuring contributions from the symmetrical stretching vibration of the carboxylate group. In particular, this band at 1425 cm^{-1} is also known as the crystal band. The band shows the crystal order of cellulose.[23] The IR spectrum of POS@ANI presented in Figure

https://doi.org/10.1021/acsomega.3c09031
ACS Omega 2024, 9, 15935−15949

2A shows both characteristic bands of Posidonia and bands corresponding to the grafts: symmetric and asymmetric stretching vibrations of C−H bonds at 2908 and 3330 cm^{-1} and C═C stretching of aniline aromatic ring at 1688 and 1596 cm^{-1}.[22] The characteristic bands of APTMS appeared at the same wavelength as those of the POS biomaterial. However, an increase in the intensity of these bands was observed for POS@ANI, confirming the grafting of silane carrying the aniline monomer. IR spectra of POS@PANI-ES and POS@PANI-EB (Figure 2B) clearly indicated the successful polymerization of aniline in the presence of the POS biomaterial. The spectra showed absorption bands at 1589 and 1486 cm^{-1}, associated with C═C stretching vibrations of the quinonoid and benzenoid rings of PANI, respectively. These two peaks confirmed the formation of the emeraldine form of PANI. The corresponding bands of the emeraldine base form were slightly shifted. This red shift can be explained by the formation of hydrogen bonds between the hydroxy groups on the surface of POS and the −NH− group of the emeraldine base. The decrease in the vibrational intensity of the benzenoid band in the POS@PANI-EB spectra is attributed to the transformation of the polaron lattice into a quinonoid structure within the polymer chain during the deprotonation process.[24]

^{13}C CP-MAS NMR spectroscopy is the most effective method for the characterization of the lignocellulosic and polymeric materials and can provide detailed information directly on the solid sample. A typical example of ^{13}C NMR spectra of POS and POS@PANI-EB are shown in Figure 3.

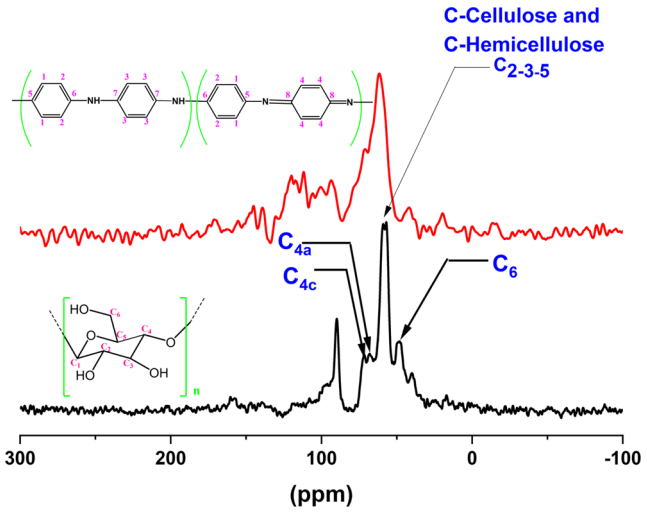

Figure 3. ^{13}C MAS NMR spectra of POS (black) and POS@PANI-EB (red spectrum).

The solid-state ^{13}C NMR spectrum of the POS exhibits strong signals of carbons in the range of 20−190 ppm, which mainly correspond to the different carbons of cellulose, hemicellulose, and lignin components of Posidonia fibers. The strong signals in the region between 50 and 107 ppm are attributed mainly to the different carbons of cellulose and hemicelluloses.[25] Nevertheless, the NMR technique is able to differentiate the crystalline versus the paracrystalline domains since the carbons located within the interior crystalline regions have a distinct chemical shift from the carbons located on the crystal surfaces or paracrystalline domains. Cellulose consists of crystalline and noncrystalline phases in different ratios, depending on its natural source. The only signal that can be mainly assigned to lignin is at 56 ppm, belonging to the methoxy group of the aromatic moieties. In addition, the region between 106 and 180 ppm is specific for the aromatic carbons of lignin. The ^{13}C CP-MAS NMR analysis of POS@PANI-ES (Figure 3) showed, in addition to the characteristic peaks of POS, a broad peak (110−160 ppm) composed of several resonances characteristic of reduced polyaniline form.[26] In particular, the peak at 153 ppm corresponds to the carbon atom in the quinoid ring, which cannot rotate around the bent bond of the imine group (═N−) in the idealized repeating unit of PANI. The peaks at 155 and 157 ppm indicate the polycondensation of the aniline, which confirms the immobilization of the PANI layer on the surface of the POS biomaterial. The characteristic peaks of POS shifted in the POS@PANI-EB spectra because of the interaction between the functional surface of POS and PAN-EB chains.

Thermogravimetric analysis was used to estimate the surface density of POS@ANI, POS@PANI-EB, and POS@PANI-ES materials (Figure 4). The TGA patterns of POS@ANI showed a slight mass loss from 100 to 200 °C, corresponding to the evaporation of moisture. The main mass loss occurred between 250 and 600 °C, attributed to the thermal decomposition of the organic phase composed of hemicellulose (the most thermally unstable compound), cellulose from the POS biomaterial, and the silane grafts (Figure 4A). The TGA of POS@PANI-EB and POS@PANI-ES (Figure 4B) shows a single broad step, corresponding to the thermal decomposition of the entire organic content of POS and the polyaniline surface-grafted materials. The mass loss attributed to PANI was determined as the difference between the two mass losses of POS@PANI and POS@ANI. The thermal decomposition of POS@PANI-EB and POS@PANI-ES extended up to 900 °C. The mass loss due to the grafted organic layer was estimated considering that thermal cleavage occurred at the functional surface bond, the molar mass of the lost moiety of APTMS, $-(CH_2)_3-NH-C_6H_5$, was $M_{mol}(APTMS) = 134\ g\ mol^{-1}$, and the surface density (SD) was calculated as

$$SD\ (mol \cdot g^{-1}) = \frac{\frac{m(POS@ANI)}{100 - m(POS@ANI)} - \frac{m(POS)}{100}}{M_{mol}(APTMS)} \quad (4)$$

The surface density of PANI was calculated from the mass loss of POS@PANI-EB and POS@PANI-ES, which corresponded to a mean aniline polymerization degree of 4. The determination of the surface density of POS@PANI is written as

$$SD = \frac{M(POS@PANI) - M(POS@ANI)}{100 \times M_{mol}(\text{grafted PANI})} \quad (5)$$

where $M(POS@PANI)$ is the mass loss of POS@PANI, $M(POS@ANI)$ is the mass loss of POS@ANI, and M_{mol}(grafted PANI) is the molar mass of the average repeat units of grafted aniline.

Elemental analyses confirmed the presence of the organic silane group and polyaniline polymers in the POS@ANI and POS@PANI materials. The surface density of aniline was calculated by determining the mass percents of carbon and nitrogen in the grafted POS materials (eqs 6 and 7):

$$SD\ (mol \cdot g^{-1}) = \frac{\%C}{100 \times nC \times 12} \quad (6)$$

https://doi.org/10.1021/acsomega.3c09031
ACS Omega 2024, 9, 15935−15949

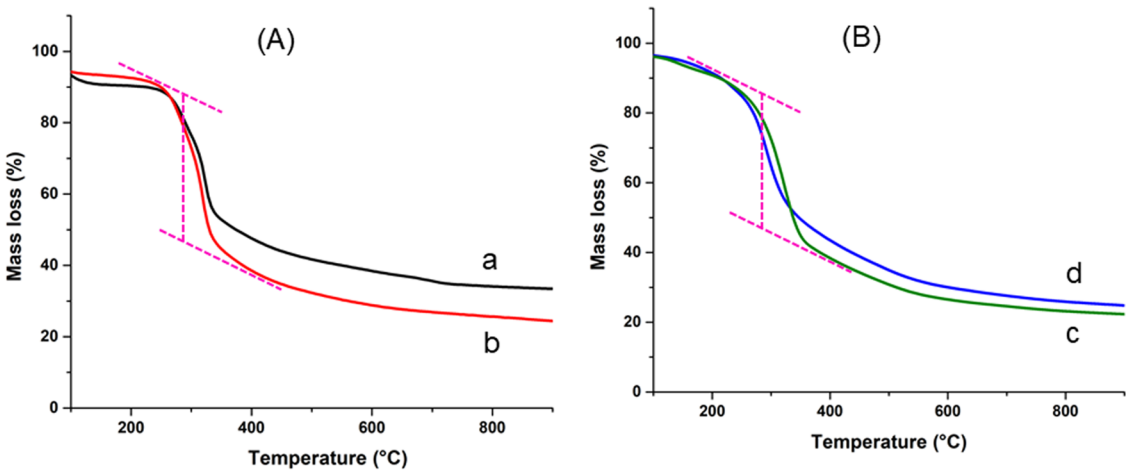

Figure 4. TGA thermograms of (A) POS (a) and POS@ANI (b) and (B) POS@PANI-ES (c) and POS@PANI-EB (d).

Table 2. Surface Density of Grafts for POS@ANI, POS@PANI-EB, and POS@PANI-ES Determined from TGA and Elemental Analysis

	EA				TGA	
materials	%C	%N	SD (C) (mmol g^{-1})	SD (N) (mmol g^{-1})	mass loss (%)	SD (mmol g^{-1})
POS	39.75	0.91			49.09	
POS@ANI	47.60	8.26	6.50	5.25	55.08	5.91
POS@PANI-ES	50.48	8.65	0.72	0.69	74.07	0.64
POS@PANI-EB	49.92	8.56	0.58	0.53	75.08	0.54

$$\text{SD}\ (\text{mol}\cdot g^{-1}) = \frac{\%N}{100 \times nN \times 14} \quad (7)$$

The surface density of aniline in the POS@ANI grafts (Table 2) is close to the theoretical density of a densely packed monolayer of aniline molecules (estimated to be between 2000 and 5000 μmol g^{-1}).[27,28] This dismissed the possible formation of a thick polysiloxane layer by polycondensation of the organosilane. The surface densities of PANI for POS@PANI-EB and POS@PANI-ES calculated from TGA and elemental analysis are shown in Table 2.

The crystalline structures of POS, POS@PANI-ES, and POS@PANI-EB materials were investigated by using XRD analysis (Figure 5). All samples exhibited four characteristic peaks detected at 15.22, 16.31, 22.24, and 34.70°, assigned to planes $\bar{1}10$, 110, 200, and 004 of the monoclinic lattice of type I cellulose, respectively.[29] The peak observed in the POS pattern at $2\theta = 29°$ is attributed to mineral impurities that are largely presented in sea biomass.[23] A supplementary peak was observed in the POS@PANI-ES pattern at 25.33° (110 plane, interplanar distance of 5 Å) corresponding to PANI in its emeraldine form.[30] Moreover, the absence of the peak at $2\theta = 29°$ indicated the total removal of mineral impurities after acidic treatment in the polymerization medium. Finally, the diffraction peaks of POS@PANI-ES and POS@PANI-EB were slightly narrower and sharper than those for the pristine POS, indicating an increase in crystallinity after prolonged immersion in the acidic polymerization medium.

The pH is a crucial parameter in the adsorption process because it strongly influences the charges of the molecules in the solution and the surface charge of the adsorbent. The ζ-potential of POS, POS@PANI-EB, and POS@PANI-ES was measured as a function of pH, providing the isoelectric point or point of zero charge (pH_{PZC}) of the materials (Figure 6). The determination of pH_{PZC} is essential for understanding the

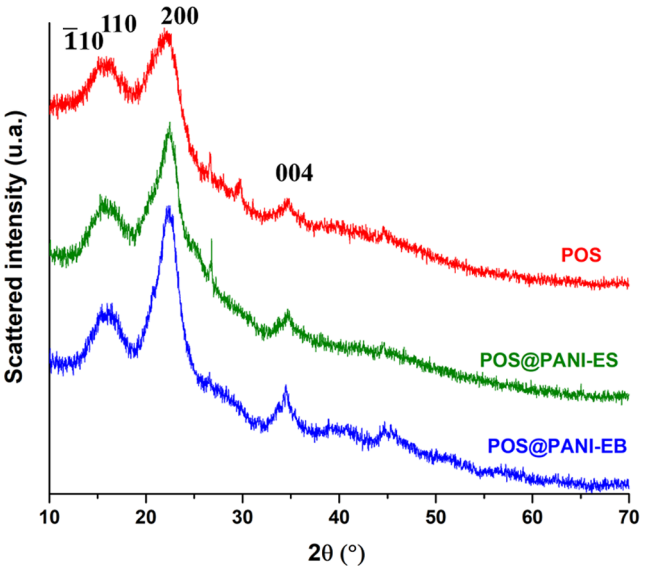

Figure 5. XRD patterns of POS, POS@PANI-EB, and POS@PANI-EB.

adsorption process, especially when electrostatic forces are involved, as is the case with the PANI polymer. The isoelectric point of POS@PANI-ES was determined to be $pH_{PZC} = 6.4$, which is significantly different from the isoelectric point of the unmodified POS biomaterial ($pH_{PZC} = 2$). This pH_{PZC} value is consistent with that of the pure emeraldine salt form of PANI,[31] confirming that the outer surface of the material is indeed composed of PANI under its emeraldine salt form coating the entire surface of the POS biomaterial. These results indicate that the surface charge of POS coated with PANI is positive for pH < 6.4 and negative for pH > 6.4. Moreover, it is

https://doi.org/10.1021/acsomega.3c09031
ACS Omega 2024, 9, 15935−15949

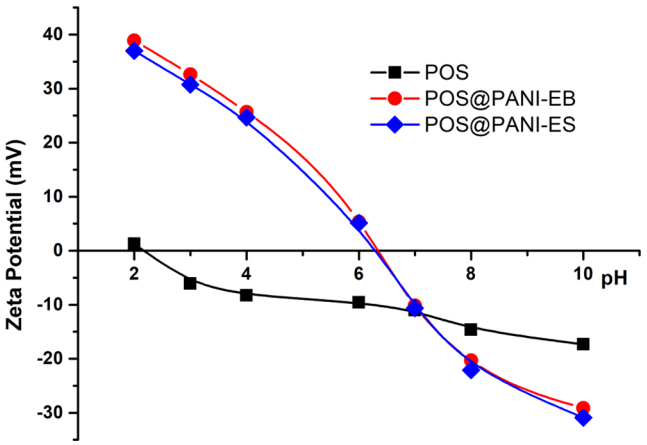

Figure 6. ζ-Potential of POS, POS@PANI-ES, and POS@PANI-EB as a function of pH.

worth noticing that POS@PANI-EB and POS@PANI-ES have the same surface charge at a given pH because POS@PANI-EB converts to POS@PANI-ES in an acidic environment through proton doping, and conversely, POS@PANI-ES transforms into POS@PANI-EB in a basic environment through dedoping. The ζ-potential data of POS@PANI-EB and POS@PANI-ES of Figure 6 are superimposed for this reason. Therefore, all of the present adsorption experiments were performed by dispersing the POS@PANI-EB and POS@PANI-ES in pure water given their ionic form is kept.

PSP adsorption to Posidonia coated with PANI and other sorbents is expected to be considerably influenced by its ionization state. Indeed, PSP is a complex organic compound having several ionizable functional groups. Phenol red has two pK_a and hence can exist in three ionic forms, cationic, zwitterionic, or anionic, under acidic, neutral, and alkaline conditions, respectively, as shown in Figure 7. At a low pH, this dye is zwitterionic, with the ketone group being protonated and a negative charge on the sulfate group. Over the pH range 6.8−8.2, the ketone group is deprotonated, resulting in an overall negative charge of PSP. Aqueous speciation of PSP was also considered following the reactions below that show all its possible solution species (eqs 8−10):

$$PSP_T \rightleftarrows +PSP^0 + PSP^- + PSP^{2-} \quad (8)$$

$$PSP^0 \rightleftarrows PSP^- + H^+ \quad (9)$$

$$PSP^- \rightleftarrows PSP^{2-} + H^+ \quad (10)$$

The specific surface area was measured by nitrogen adsorption experiments at 77 K according to the BET method (Figure 8). The adsorption and desorption branches were

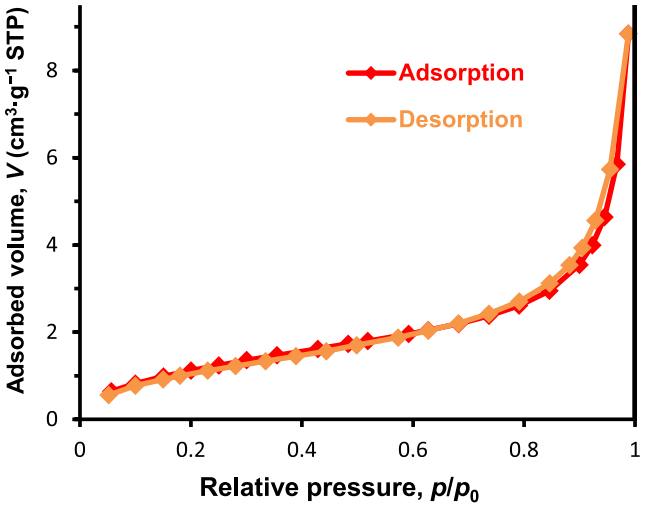

Figure 8. BET nitrogen adsorption and desorption isotherms of POS@ANI.

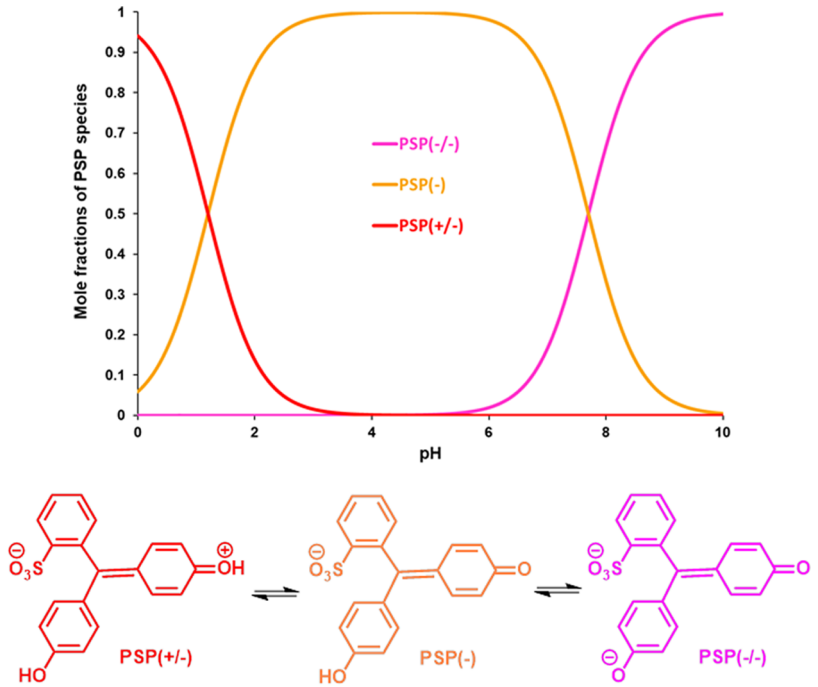

Figure 7. Structure and pH-dependent speciation of PSP. The graph is plotted using the log(K_a) values of PSP, where PSP(±), PSP(−), and PSP(−/−) represent the different species of PSP.

https://doi.org/10.1021/acsomega.3c09031
ACS Omega 2024, 9, 15935−15949

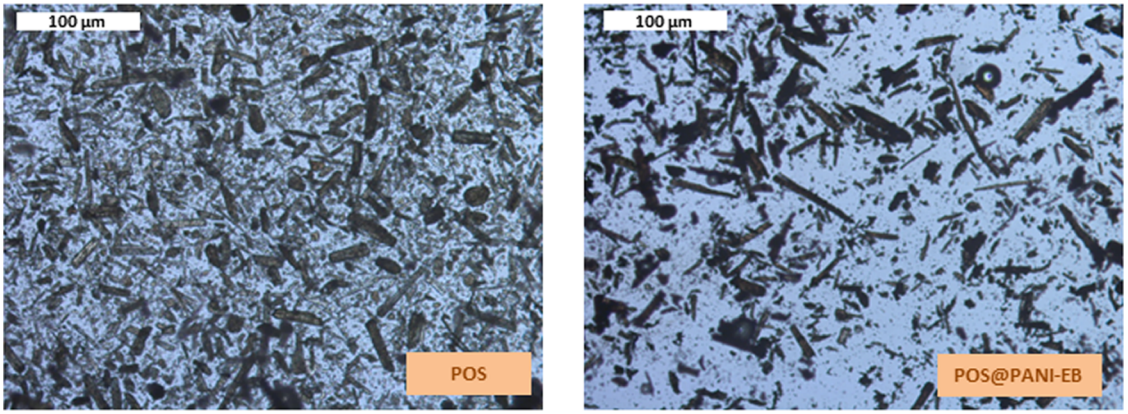

Figure 9. Optical microscopy pictures of POS and POS@PANI-EB in water.

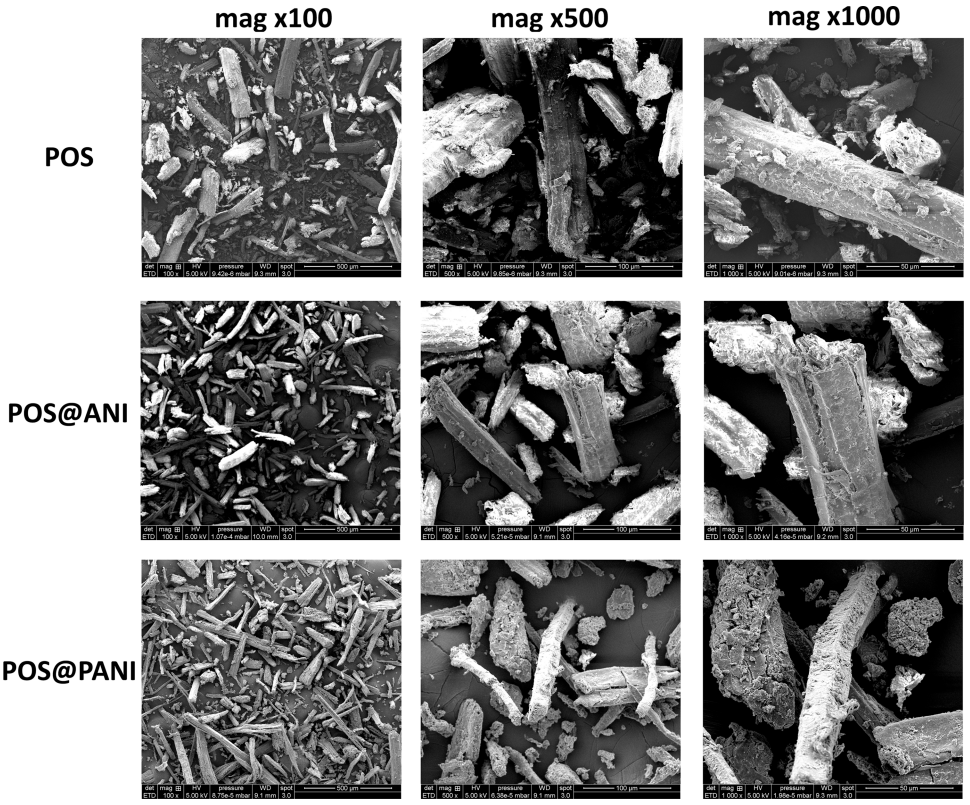

Figure 10. SEM pictures of POS, POS@ANI, and POS@PANI powders at three magnifications ×100, ×500, and ×1000.

superimposed, showing that there is negligible mesoporosity. There is no significant microporosity detected in a *t*-plot. The specific surface area determined from the BET equation in the relative pressure range p/p_0 = 0.05−0.30 was 1.1 $m^2\ g^{-1}$ for POS, 4.7 $m^2\ g^{-1}$ for POS@ANI, and 4.0 $m^2\ g^{-1}$ for POS@PANI-ES. The specific surface area of pristine POS was quite low. Grafting the organosilane increased the specific surface area, probably because of the roughness of the grafted layer. Finally, copolymerization of aniline giving POS@PANI-ES kept the specific surface area as its measured decrease was small and rather insignificant.

The morphology of POS and POS@PANI-EB was studied by optical microscopy. Different dispersions of POS and POS@PANI-EB in water were observed (Figure 9). POS material showed individual fibers with regular shape and clear and smooth surface. The approximate fiber length is 30−50 μm with a width of 17 μm. After the three chemical modification steps, the size of POS@PANI-EB remained constant, demonstrating the stability of the morphology of the material throughout the modification process.

Scanning electron microscopy (SEM) provided higher-resolution pictures that supplemented optical microscopy. SEM pictures of POS, POS@ANI, and POS@PANI powders (Figure 10) revealed the same pieces of fibers as optical microscopy. Pictures at higher magnification showed the surface morphology to be essentially smooth with some crazes and a few protruding lumps of amorphous material. Grafting aniline and growing polyaniline strands at the surface did not change the morphology. Indeed, the grafting process yields a thin PANI layer. Possible adhesion of PANI particles (coming from homopolymerization of aniline in aqueous solution) on POS fibers has not been observed.

https://doi.org/10.1021/acsomega.3c09031
ACS Omega 2024, 9, 15935−15949

3.2. Performance for Adsorption of Phenol Red.

3.2.1. Influence of Adsorbent Quantity. Different amounts of adsorbent from 6 to 22 mg dispersed in 5 mL of aqueous medium were investigated. From the histogram shown in Figure 11, it can be seen that when using a mass of 18 mg of

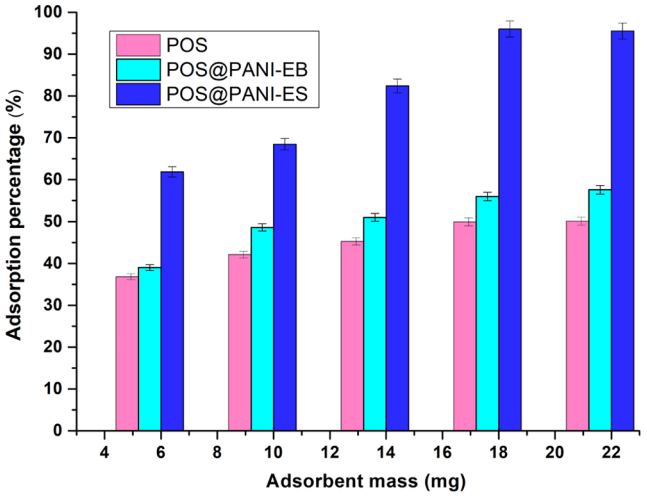

Figure 11. Mass effect of native and modified Posidonia materials on adsorption of the PSP aqueous solution. Solution volume = 5 mL; concentration = 50 μmol L^{-1}; contact time = 60 min; and temperature = 298 °K.

POS@PANI-ES, the maximum capacity for the uptake of the PSP dye reaches approximately 96%. This performance is significantly superior to that of the other POS materials used, which show uptake capacities in the range of 45 to 55%. To maintain a congruent number of available adsorption sites, it is essential to match the fixed amount of PSP to the adsorbent distribution in the solution. Above a certain mass threshold, there is a slight decrease in the adsorption rate. This decrease may indicate the presence of a supplementary interaction between PSP molecules and native or modified Posidonia bioadsorbents. A competitive interplay between material particles containing PSP fractions and free adsorbents may be responsible for this phenomenon. Therefore, it is advisable to use an adsorbent mass of ≤18 mg. This avoids ineffective overdosing. An adsorbent mass of 18 mg was selected for future studies focusing on the determination of adsorption capacity by saturation of all accessible sites.

3.2.2. Adsorption Kinetics. Adsorption kinetics is a critical parameter for evaluating the effectiveness of an adsorbent. The objective was to compare the adsorption performance between PANI-EB and PANI-ES grafted onto the surface of Posidonia, considering their distinct characteristics, particularly different surface charges. This comparison offers valuable insights into the adsorption behavior of these materials, enhancing our understanding of their potential applications in wastewater treatment. The impact of contact time on PSP adsorption onto POS@PANI-EB and POS@PANI-ES at different concentrations of PSP (5×10^{-5} and 10^{-4} mol L^{-1}) was measured in adsorption kinetics experiments using the depletion method (Figure 12). At the tested PSP concentrations, the adsorption uptake of PSP onto the POS@PANI-ES material was significantly higher compared to the POS@PANI-EB material during the adsorption equilibration period. Indeed, the binding to POS@PANI-ES material was remarkably fast, increasing from 85% in 2 min to 97% in 15 min, while POS@PANI-EB enhanced from 25% in 2 min to 50% after 15 min of contact time. Such variation in mass transfer rate can be attributed to the nature of the interaction involved: the adsorption on POS@PANI-ES relies on an electrostatic interaction, whereas in the case of POS@PANI-EB, it is influenced by hydrogen bond formation. A typical time scale taken from the scarce experimental data is indeed much shorter than the typical time spanning from minutes to hours.[32]

Kinetic models were applied to evaluate the experimental results for POS@PANI-ES and POS@PANI-EB. Commonly used models for assessing the adsorption mechanism include the pseudo-first-order[33] and pseudo-second-order[34] models (Figure 13).

The pseudo-first-order model, established by Lagergren, describes the adsorption kinetics where the rate is first order with respect to the surface concentration of available adsorption sites.[35] The adsorption rate at time t is proportional to the difference between the amount adsorbed at equilibrium ($Q(\infty)$) and the amount adsorbed at time t ($Q(t)$) (eqs 11 and 12):

$$\frac{dQ(t)}{dt} = k_1[Q(\infty) - Q(t)] \tag{11}$$

Integration of eq 11 using $Q(0) = 0$ gives

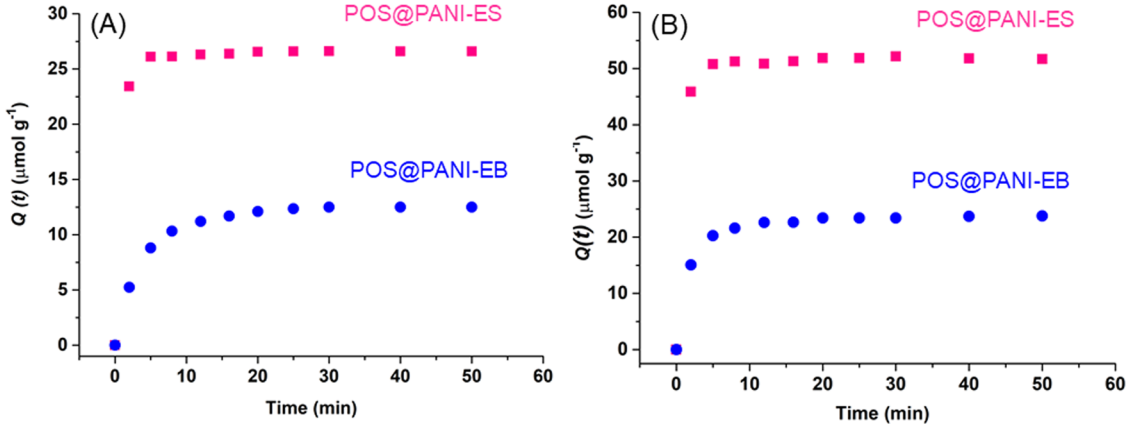

Figure 12. Adsorption kinetics experiments onto POS@PANI-EB and POS@PANI-ES from PSP solution at concentrations of (A) 50 μmol L^{-1} and (B) 100 μmol L^{-1} at 298 K.

https://doi.org/10.1021/acsomega.3c09031
ACS Omega 2024, 9, 15935−15949

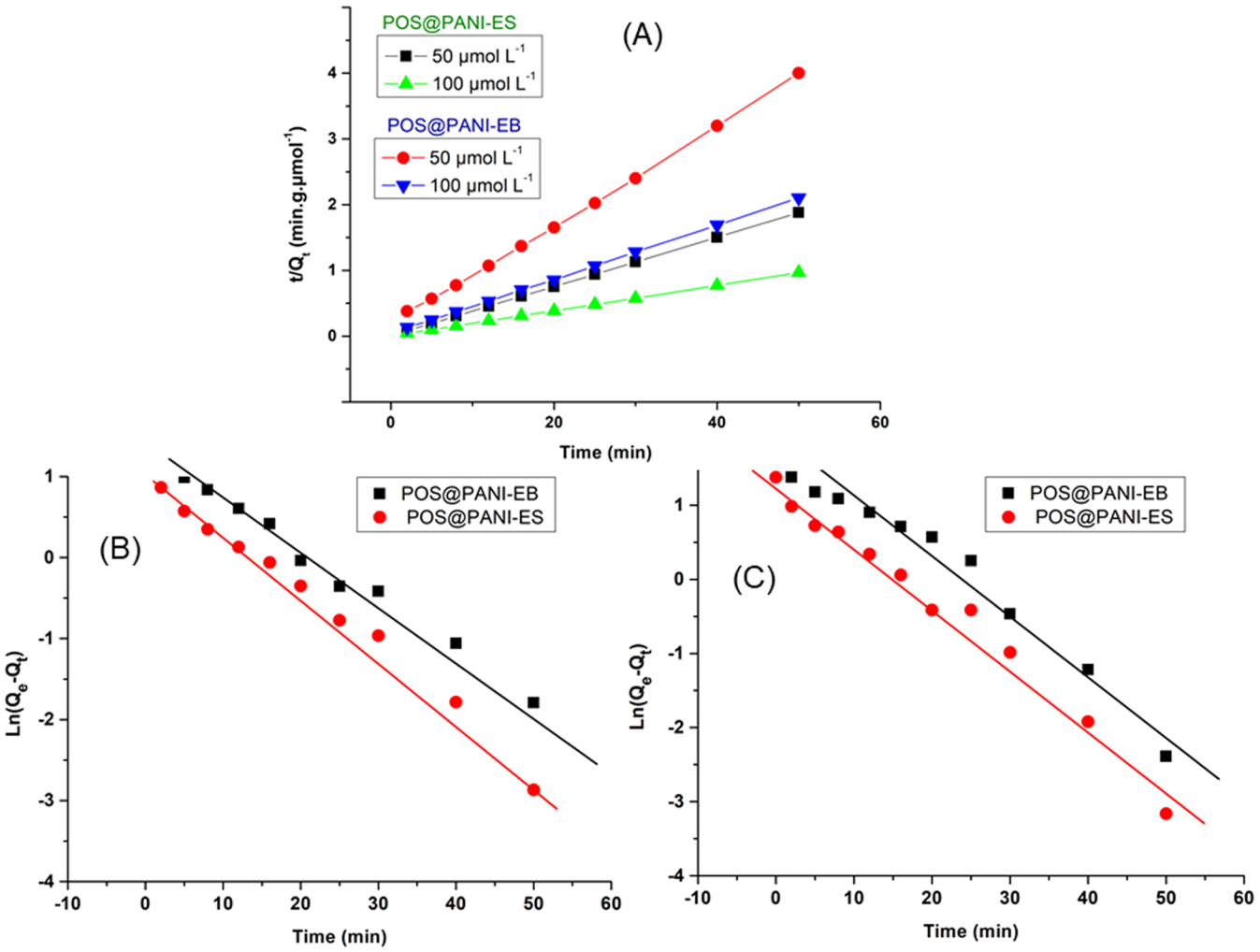

Figure 13. (A) Pseudo-second-order kinetics model for adsorption of PSP onto POS@PANI-ES and POS@PANI-EB at concentrations 50 and 100 μmol L^{-1}. Pseudo-first-order kinetics model for adsorption of PSP onto POS@PANI-ES and POS@PANI-EB at concentrations (B) 50 μmol L^{-1} and (C) 100 μmol L^{-1}.

Table 3. Kinetic Parameters of the Pseudo-First-Order and Pseudo-Second-Order Models of the Adsorption Study of PSP onto POS@PANI-ES and POS@PANI-EB Materials

			pseudo-first-order model			pseudo-second-order model		
materials	C_0 (μmol L^{-1})	$Q_{e,exp}$ (μmol g^{-1})	k_1	$Q_{e,calc}$ (μmol g^{-1})	R^2	k_2	$Q_{e,calc}$ (μmol g^{-1})	R^2
POS@PANI-ES	50	26.6	0.061	25.3	0.991	0.010	24.3	0999
	100	51.6	0.055	55.9	0.966	0.012	52.1	0.999
POS@PANI-EB	50	12.5	0.084	11.1	0.989	0.032	13.2	0.999
	100	23.8	0.083	25.3	0.981	0.040	24.3	0.999

$$\ln[Q(\infty) - Q(t)] = \ln[Q(\infty)] - k_1 t \quad (12)$$

where k_1 (min^{-1}) is the kinetic constant of pseudo-first order, and $Q(\infty)$ and $Q(t)$ are the adsorbed amounts at equilibrium and a given time t.

The nonlinear form of the pseudo-second-order adsorption rate equation, as introduced by Blanchard,[36] is frequently employed to describe the binding kinetics of ions to solid supports.[34] This equation can be expressed as follows:

$$\frac{dQ(t)}{dt} = k_2[Q(\infty) - Q(t)]^2 \quad (13)$$

Integration of eq 13 using $Q(0) = 0$ yields

$$\frac{t}{Q(t)} = \frac{1}{k_2 Q(\infty)^2} + \frac{1}{Q(\infty)} \quad (14)$$

where k_2 (g μmol^{-1} min^{-1}) is the kinetic constant of pseudo-second order and $Q(\infty)$ and $Q(t)$ are the adsorbed amounts at equilibrium and a given time t.

According to the data in Table 3, the rate constants for the pseudo-first-order and pseudo-second-order models of POS@PANI-ES were lower than those found for POS@PANI-EB. Nevertheless, from the pseudo-second-order model, it is evident that the adsorption on POS@PANI-ES occurs approximately 3 to 5 times faster than on POS@PANI-EB, further supporting the application of the adsorption process using biomaterials for wastewater decontamination, which

https://doi.org/10.1021/acsomega.3c09031
ACS Omega 2024, 9, 15935−15949

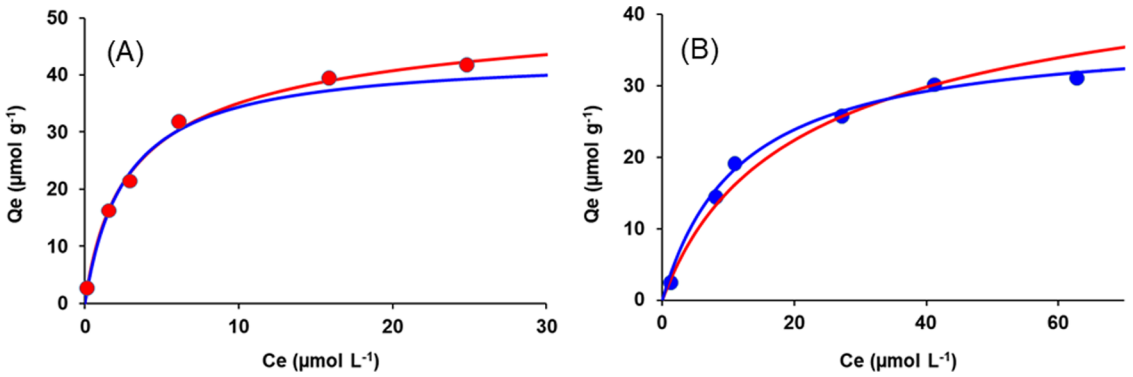

Figure 14. Adsorption isotherms and best nonlinear fits of the adsorption models (red: Volmer model; blue: Langmuir model) to experimental PSP adsorption (A) POS@PANI-ES and (B) POS@PANI-EB.

indeed requires rapid adsorption to allow a short operating time of the process and high efficiencies to remove organic pollutants. The fast kinetic processes observed in the case of POS@PANI-EB result from the presence of its positive charge, which enhances its attraction to negatively charged molecules, promoting interactions through electrostatic forces. In contrast, the absence of a positive charge in POS@PANI-ES decreases its attraction to negatively charged particles, relying more on weaker hydrogen bonding interactions. In addition, the values of adsorption uptake at equilibrium calculated from the pseudo-second-order model and the pseudo-first-order model are closer to the experimental values. Thus, the pseudo-second-order model was considered as better than the pseudo-first-order kinetic model because it was closer fitted to the experimental data ($R^2 > 0.99$). Similar kinetic behavior was also observed for the adsorption of dyes on polyaniline-coated filter paper.[37]

3.2.3. Adsorption Isotherms. The adsorption isotherm is a well-established tool for describing the interactive relationship between the adsorbent and adsorbate over a range of concentrations. Experimental isotherm data are also used to describe the adsorbent surface affinity and properties. Equilibrium adsorption isotherms were measured for the adsorption of PSP on POS@PANI-EB and POS@PANI-ES after an equilibration time of 60 min. Their analysis using thermodynamic models was done with the Langmuir and Volmer theoretical models. The Langmuir isotherm is a classical model that considers homogeneous and independent binding sites on the surface of the adsorbent. Maximum adsorption is achieved when all sites are occupied, resulting in a plateau in the adsorption isotherm. The underlying assumptions of the Langmuir model are satisfied for the localized adsorption of PSP on the adsorption sites. The Langmuir adsorption isotherm for adsorption site on adsorbent assumes its classical form as follows:[38]

$$Q_e = Q_{max}\frac{KC_e}{1 + KC_e} \tag{15}$$

where Q_e (mol g^{-1}) is the adsorbed density in equilibrium with a solution of concentration C_e (mol L^{-1}) described by two parameters, the maximum adsorption capacity Q_{max} corresponding to the density of adsorption sites, and the adsorption equilibrium constant K considered as a quasi-chemical equilibrated reaction of adsorbing molecules and surface sites.

The Volmer model is based on the same assumptions as those given by the Langmuir model regarding the energy homogeneity of the adsorbent surface and the absence of interactions between the adsorbed molecules. This model describes adsorption on a surface for nonlocalized (mobile) adsorption isotherm. The adsorbed molecules can diffuse freely on the surface, which makes a difference with the Langmuir model. The Volmer equation is written according to the following expression:[39]

$$C_e = \frac{1}{K}\frac{\theta}{1-\theta}e^{\theta/1-\theta} \tag{16}$$

where θ is the surface coverage, $\theta = Q_e/Q_{max}$, and K is the binding constant for adsorption equilibrium. The Volmer isotherm differs from the Langmuir one by the supplementary term $e^{\theta/(1-\theta)}$. This relationship in the form of C_e as a function of Q_e was inverted into Q_e as a function of C_e by the numerical resolution of eq 16.

The Langmuir and the Volmer adsorption isotherms were fitted to the experimental data by minimizing the average relative error function (ARE, eq 17) by nonlinear regression.

$$\mathrm{ARE} = \frac{1}{n-p}\sum_{i=1}^{n}\left|\frac{Q_{exp} - Q_{calc}}{Q_{exp}}\right| \tag{17}$$

where n and p are the number of data points and fitted parameters, respectively, and Q_{exp} and Q_{calc} are the experimental and fitted adsorption capacities at equilibrium, respectively.

As an important feature, modeling experimental adsorption data allows discrimination of the mechanisms of adsorption and the related physicochemical interactions. The models of Volmer and Langmuir were fitted to the experimental adsorption isotherms of POS@PANI-ES and POS@PANI-EB. The result is a thermodynamic description of the adsorption process regarding Q_{max} and K parameters for the two adsorbents. So, the difference in adsorption behavior can come either from a different nature of the sites via an increase in Q_{max}, or from a higher affinity for the adsorption sites via an increase of K value. Experimental adsorption isotherms at 298 K and the best fit of the suitable model are given for POS@PANI-ES and POS@PANI-EB in Figure 14. The thermodynamic parameters are given in Table 4. The Volmer model fitted more accurately the experimental adsorption isotherm of PSP to POS@PANI-ES, whereas the Langmuir model was preferred for POS@PANI-EB. Therefore, the PSP molecules adsorbed on POS@PANI-ES are mobile because electrostatic adsorption prevails. Because electrostatic interactions are long-

https://doi.org/10.1021/acsomega.3c09031
ACS Omega 2024, 9, 15935−15949

Table 4. Parameters of the Best Fits of the Volmer and Langmuir Models to Experimental Adsorption Isotherms of PSP to POS@PANI-EB and POS@PANI-ES at 298 K

	POS@PANI-ES			POS@PANI-EB		
models	log(K)	Q_{max} (μmol g^{-1})	ARE	log(K)	Q_{max} (μmol g^{-1})	ARE
Langmuir isotherm	2.57	43.5	0.09	3.89	37.8	0.03
Volmer isotherm	3.29	71.5	0.03	3.02	57.23	0.22

ranged, adsorbed PSP molecules are not necessarily in close contact with the cationic sites. PSP molecules can jump from one cationic site to another without having to overcome an energy barrier because the high density of cationic groups makes the sites close to each other and electrostatic interactions being nonlocalized. Conversely, adsorption on POS@PANI-EB takes place at well-defined sites, mostly the neutral quinone-diimine units. Adsorption requires a close contact of PSP molecules to these functional groups that behave as discrete independent binding sites, therefore meeting the assumptions of the Langmuir model. The thermodynamic modeling of adsorption onto POS@PANI-ES and POS@PANI-EB provided the parameters Q_{max} and K for the positively charged groups of PANI-ES and the quinone-diimine unit PANI-EB binding sites grafted onto the POS biomaterial. The binding affinity was higher for POS@PANI-ES due to the stronger interaction of PSP with the electrical charges of PANI-ES (mobile adsorption). This enhanced affinity is attributed to the anion exchange between the sulfonic group of PSP and chloride ions of the positively charged groups of the PANI-ES surface. The higher affinity of PSP compared to that of chloride may be attributed to its more hydrophobic nature. In contrast, the adsorption of PSP on POS@PANI-EB is driven by nonelectrostatic interactions, coming from hydrogen bonding interactions between the quinone-diimine and amine groups of PANI-EB and the phenolic group of PSP, which can be considered localized adsorption sites.

3.2.4. Comparison of the Adsorption Capacity of Different Adsorbents. In the field of wastewater treatment and environmental remediation, various bioadsorbents have been extensively studied for their efficacy in removing pollutants from aqueous solutions. Table 5 presents a comprehensive comparison of the adsorption capacities reported in the literature for different adsorbents. Activated carbon, a widely used adsorbent known for its high surface area and porous structure, demonstrates excellent adsorption capacities for organic pollutants.[41,42] Biomass wastes hold great promise due to their abundance, renewability, and cost-effectiveness. Their adsorption capabilities make them valuable candidates for sustainable and eco-friendly approaches to wastewater treatment. Among these, *Ficus carica* bast, the sea plant *P. oceanica* L., and dead leaves of oak trees have shown notable adsorption capacities for various pollutants.[43,44] Agricultural byproducts, such as corn silk, coconut shells, and rice husks, have gained attention due to their cost-effectiveness and abundant availability, exhibiting notable adsorption capacities for a range of pollutants.[45−47] These agricultural wastes have been utilized as renewable sources for the production of adsorbents, offering an alternative to traditional activated carbon. Moreover, food wastes, such as chicken eggshell beads, lemon peel, and almond shell, exhibit unique adsorption properties for both cationic and anionic dyes, showcasing their potential applications in environmental remediation.[48−50] The adsorption capacity of *P. oceanica* L. coated with polyaniline emeraldine salt forms is consistent with these diverse adsorbents, demonstrating its efficacy in the removal of pollutants from aqueous solutions.

Table 5. Comparison of Several Adsorbent Capacities for Dye Removal in Aqueous Solution

materials		dye	adsorption capacity (mg g^{-1})	ref
commercial materials	activated carbon	acid yellow 23	3.32	41
	nanoactivated carbon	methylene blue	28.09	42
biomass wastes	*F. carica* bast	methylene blue	55.56	43
	sea plant (*P. oceanica* L.)	methylene blue	27.78	44
	dead leaves of oak trees	crystal violet	31.65	44
agriculture wastes	corn silk	reactive blue 19	60.60	45
	coconut shells	methylene blue	106.40	46
	rice husks	congo red	1.58	47
food wastes	chicken eggshell beads	reactive blue 4	24.10	48
	lemon peel	reactive blue 4	2.59	49
	almond shell	crystal violet	12.20	50

3.3. Effect of Ionic Strength. To investigate the influence of electrolytes in solution on the adsorption of PSP onto POS@PANI-ES, varying quantities of NaCl or $CaCl_2$ were introduced into the aqueous PSP solution with an initial concentration of C_0 = 0.25 mmol L^{-1}. The presence of inorganic salts in the solution greatly decreases the adsorption of PSP, with the two salts exhibiting almost identical effects (Figure 15). The amount of PSP adsorbed goes from 96% in the absence of added salts to approximately 42% with an added ionic strength of 0.40 mol L^{-1}. Beyond 0.40 mol L^{-1}, the quantity of adsorbed PSP onto POS@PANI-ES remains constant. The observed reduction in PSP adsorption on POS@PANI-ES material in the presence of various electrolytes can be rationalized by competitive adsorption, where inorganic

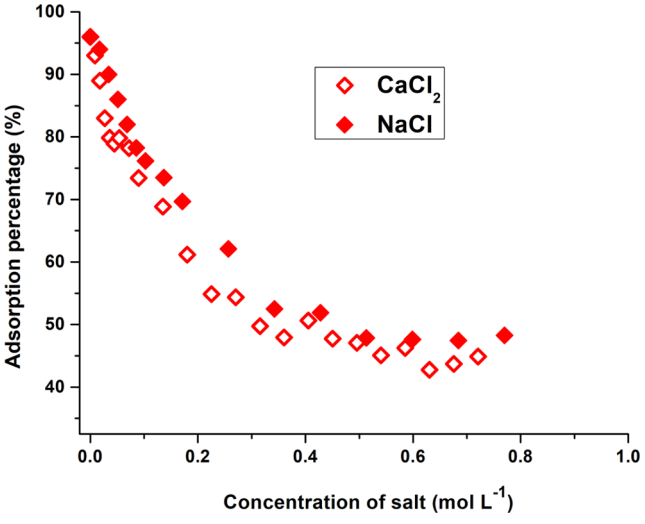

Figure 15. Adsorbed fraction of PSP onto POS@PANI-ES material in the presence of NaCl and $CaCl_2$ salts; initial concentration of PSP C_0 = 0.25 mmol L^{-1}.

https://doi.org/10.1021/acsomega.3c09031
ACS Omega 2024, 9, 15935−15949

anions and PSP compete for surface sites on the adsorbent.[40] Indeed, salts such as sodium chloride (NaCl) and calcium chloride ($CaCl_2$) can disturb the favorable electrostatic interactions between the cationic polymer PANI and the PSP molecules. This competitive dynamic leads to a noticeable decrease in the accessibility of adsorption sites for PSPs, leading to an overall reduction in adsorption efficiency. In addition, the presence of salts can form an electrostatic barrier around adsorption sites, further undermining the interaction between the positive charges of the cationic polymer and the negative charges of the PSP molecules. These effects of ionic strength on the PSP adsorption process can pose a challenge when using POS@PANI-ES materials in water treatment. Indeed, these contain different salts that affect the adsorption capabilities of the materials. However, these materials can be affected by various salts which influence their adsorption capacities. Nevertheless, in water treatment scenarios, water is generally considered to have high salinity when the NaCl concentration is around 0.06 mol L^{-1} and PSP remains approximately 80% adsorbed at this concentration, a level considered suitable for systems with robust adsorption capacities.

4. CONCLUSIONS

The adsorption properties of phenol red dye on Posidonia surface modified with polyaniline emeraldine salt, prepared by oxidative copolymerization in acidic medium, were compared with those of Posidonia grafted with polyaniline emeraldine base. Favorable performances of such a material were revealed as fast adsorption kinetics and high adsorption efficiency for PSP. The simple comparison of adsorbed amounts of PSP molecules showed that both POS@PANI-ES and POS@PANI-EB materials could bind more PSP than the unmodified Posidonia. Modeling the adsorption isotherm allowed us to separate the affinity contributions of the polyaniline sites for PSP. The data from the isothermal experiments of POS@PANI-EB fit well with the Langmuir model, which takes into account the presence of a localized type of adsorption sites, while the adsorption on POS@PANI-ES was in agreement with the Volmer model, which takes into account the mobility of the adsorbate at positively charged sites of the polyaniline salt. The presence of inorganic salts significantly affects the adsorption of PSP on POS@PANI-ES. Competitive adsorption between ions and PSP, in addition to disrupted electrostatic interactions caused by salts, leads to a reduced adsorption efficiency. While this underscores the importance of considering ionic strength, the promising performance of POS@PANI-ES materials in water treatment is evident within an optimal salinity range. This highlights their potential as versatile and effective adsorbents to address water pollution challenges.

AUTHOR INFORMATION

Corresponding Author

Souhaira Hbaieb − *Laboratoire de Recherche: Caractérisations, Applications et Modélisation de Matériaux, Université de Tunis El Manar, Faculté des Sciences de Tunis, Tunis 2092, Tunisia;* orcid.org/0000-0003-2565-5970; Email: souhaira.hbaieb@fst.utm.tn

Authors

Karima Ferchichi − *Laboratoire de Recherche: Caractérisations, Applications et Modélisation de Matériaux, Université de Tunis El Manar, Faculté des Sciences de Tunis, Tunis 2092, Tunisia*

Amaini Chouchaine − *Laboratoire de Recherche: Caractérisations, Applications et Modélisation de Matériaux, Université de Tunis El Manar, Faculté des Sciences de Tunis, Tunis 2092, Tunisia*

Noureddine Amdouni − *Laboratoire de Recherche: Caractérisations, Applications et Modélisation de Matériaux, Université de Tunis El Manar, Faculté des Sciences de Tunis, Tunis 2092, Tunisia*

Yves Chevalier − *Laboratoire d'Automatique, de Génie des Procédés et de Génie Pharmaceutique, Université de Lyon 1, 69622 Villeurbanne, France;* orcid.org/0000-0002-7526-5658

Complete contact information is available at: https://pubs.acs.org/10.1021/acsomega.3c09031

Author Contributions

All authors contributed to the study's conception and design. Material preparation, data collection, and analysis were performed by [K.F.], [A.C.], [N.A.], [Y.C.], and [S.H.]. The first draft of the manuscript was written by [K.F.], and all authors commented on previous versions of the manuscript. All authors read and approved the final manuscript.

Notes

The authors declare no competing financial interest.

ACKNOWLEDGMENTS

This work was supported by the Cross-border project Italy-Tunisia "Méthodologies d'Économie Durable pour les Déchets Côtiers Utilisables des Plages" (MEDDé.Co.U.Plages IS_3.2_086).

REFERENCES

(1) Njuguna, D. G.; Schönherr, H. Xanthan gum hydrogels as high-capacity adsorbents for dye removal. *ACS Appl. Polym. Mater.* **2021**, *3* (6), 3142−3152.

(2) Johnson, J.; Saha, E.; Chhetri, A.; Suresh, E.; Mitra, J. Self-assembled melaminium adipate lamellae for adsorptive removal of anionic dyes from wastewater. *ACS Appl. Polym. Mater.* **2021**, *3* (2), 651−660.

(3) Tang, J.; Song, Y.; Zhao, F.; Spinney, S.; da Silva Bernardes, J.; Tam, K. C. Compressible cellulose nanofibril (CNF) based aerogels produced via a bio-inspired strategy for heavy metal ion and dye removal. *Carbohydr. Polym.* **2019**, *208*, 404−412.

(4) Bryant, L. F. Water and Wastewater Infrastructure. In *Women in Infrastructure*; Layne, P.; Tietjen, J. S., Eds.; Springer: Cham, 2022.

(5) Salama, A. New sustainable hybrid material as adsorbent for dye removal from aqueous solutions. *J. Colloid Interface Sci.* **2017**, *487*, 348−353.

(6) Shaw, R.; Sharma, R.; Tiwari, S.; Tiwari, S. K. Surface engineered zeolite: an active interface for rapid adsorption and degradation of toxic contaminants in water. *ACS Appl. Mater. Interfaces* **2016**, *8* (19), 12520−12527.

(7) Gahlot, R.; Taki, K.; Kumar, M. Efficacy of nanoclays as the potential adsorbent for dyes and metal removal from the wastewater: A review. *Environ. Nanotechnol., Monit. Manage.* **2020**, *14*, No. 100339.

(8) Liu, Q.; Li, Y.; Chen, H.; Lu, J.; Yu, G.; Möslang, M.; Zhou, Y. Superior adsorption capacity of functionalised straw adsorbent for dyes and heavy-metal ions. *J. Hazard. Mater.* **2020**, *382*, No. 121040.

(9) Rahman, O.; Rahman, M. M.; Maniruzzaman, M. Removal of dye and heavy metals from industrial wastewater by activated charcoal-banana rachis cellulose nanocrystal composites filter. *Int. J. Environ. Anal. Chem.* **2022**, 1−19.

(10) Yadav, D.; Awasthi, S. K. Ni nanoparticle-immobilized imine-linked microspherical covalent organic polymer for degradation studies of organic dyes. *ACS Appl. Polym. Mater.* **2021**, *3* (11), 5460−5469.
(11) Malhotra, M.; Sudhaik, A.; Raizada, P.; Ahamad, T.; Nguyen, V.-H.; Van Le, Q.; Selvasembian, R.; Mishra, A. K.; Singh, P. An overview on cellulose-supported photocatalytic materials for the efficient removal of toxic dyes. *Ind. Crops Prod.* **2023**, *202*, No. 117000.
(12) Crini, G.; Torri, G.; Lichtfouse, E.; Kyzas, G. Z.; Wilson, L. D.; Morin-Crini, N. Dye removal by biosorption using cross-linked chitosan-based hydrogels. *Environ. Chem. Lett.* **2019**, *17* (4), 1645−1666.
(13) Rafatullah, M.; Sulaiman, O.; Hashim, R.; Ahmad, A. Adsorption of methylene blue on low-cost adsorbents: A review. *J. Hazard. Mater.* **2010**, *177* (1−3), 70−80.
(14) Solangi, N. H.; Kumar, J.; Mazari, S. A.; Ahmed, S.; Fatima, N.; Mubarak, N. M. Development of fruit waste derived bio-adsorbents for wastewater treatment: A review. *J. Hazard. Mater.* **2021**, *416*, No. 125848.
(15) Ben Douissa, N.; Bergaoui, L.; Mansouri, S.; Khiari, R.; Mhenni, M. F. Macroscopic and microscopic studies of methylene blue sorption onto extracted celluloses from *Posidonia oceanica*. *Ind. Crops Prod.* **2013**, *45*, 106−113.
(16) Ben Douissa, N.; Dridi-Dhaouadi, S.; Mhenni, M. F. Spectrophotometric investigation of the interactions between cationic (C.I. Basic Blue 9) and anionic (C.I. Acid Blue 25) dyes in adsorption onto extracted cellulose from Posidonia oceanic in single and binary system. *Water Sci. Technol.* **2016**, *73*, 2211−2221.
(17) Boubakri, S.; Djebbi, M. A.; Bouaziz, Z.; Namour, P.; Ben Haj Amara, A.; Ghorbel-Abid, I.; Kalfat, R. Nanoscale zero-valent iron functionalized *Posidonia oceanica* marine biomass for heavy metal removal from water. *Environ. Sci. Pollut. Res.* **2017**, *24*, 27879−27896.
(18) Elmorsi, R. R.; El-Wakeel, S. T.; El-Dein, W. A. S.; Lotfy, H. R.; Rashwan, W. E.; Nagah, M.; Abou-El-Sherbini, K. S. Adsorption of methylene blue and Pb^{2+} by using acid-activated *Posidonia oceanica* waste. *Sci. Rep.* **2019**, *9* (1), No. 3356.
(19) Sagharigar, T.; Baniasadi, B.; Ebadi, M.; Asri, M.; Aliabadi, M. Photocatalytic discoloration of aqueous Phenol Red solutions using TiO_2 nanocatalyst. *J. Biodiversity Environ. Sci.* **2014**, *5* (1), 336−342.
(20) Salter, C.; Langhus, D. L. The chemistry of swimming pool maintenance. *J. Chem. Educ.* **2007**, *84* (7), 1124−1128.
(21) Ayadi, C.; Anene, A.; Kalfat, R.; Chevalier, Y.; Hbaieb, S. Molecular imprints frozen by strong intermolecular interactions in place of cross-linking. *Chem. - Eur. J.* **2021**, *27*, 2175−2183.
(22) Ayadi, C.; Anene, A.; Kalfat, R.; Chevalier, Y.; Hbaieb, S. Molecularly imprinted polyaniline on silica support for the selective adsorption of benzophenone-4 from aqueous media. *Colloids Surf., A* **2019**, *567*, 32−42.
(23) Tarchoun, A. F.; Trache, D.; Klapötke, T. M. Microcrystalline cellulose from *Posidonia oceanica* brown algae: Extraction and characterization. *Int. J. Biol. Macromol.* **2019**, *138*, 837−845.
(24) Zhuravlev, N. D.; Siepmann, J. I.; Schure, M. R. Surface coverages of bonded-phase ligands on silica: A computational study. *Anal. Chem.* **2001**, *73* (16), 4006−4011.
(25) Chadlia, A.; Farouk, M. M. Chemical modification of Posidonia with cyclic anhydrides: effect on thermal stability. *Carbohydr. Res.* **2010**, *345*, 264−269.
(26) Zujovic, Z.; Kilmartin, P. A.; Travas-Sejdic, J. The applications of solid-state NMR to conducting polymers. The special case on polyaniline. *Molecules* **2020**, *25* (3), No. 444.
(27) Ping, Z. In situ FTIR−attenuated total reflection spectroscopic investigations on the base−acid transitions of polyaniline. Base−acid transition in the emeraldine form of polyaniline. *J. Chem. Soc., Faraday Trans.* **1996**, *92*, 3063−3067.
(28) Erard, J. F.; Nagy, L.; Kovats, E.s. The preparation of mixed organic layers chemically bonded on silicon dioxide. *Colloids Surf.* **1984**, *9* (2), 109−132.
(29) Pedicini, R.; Maisano, S.; Chiodo, V.; Conte, G.; Policicchio, A.; Agostino, R. G. Posidonia Oceanica and Wood chips activated carbon as interesting materials for hydrogen storage. *Int. J. Hydrogen Energy* **2020**, *45*, 14038−14047.
(30) Guo, J.; Guan, L.; Wei, H.; Khan, M. A.; Zhang, X.; Li, B.; Wang, Q.; Weeks, B. L.; Young, D. P.; Shen, T.; Wei, S.; Guo, Z. Enhanced negative magnetoresistance with high sensitivity of polyaniline interfaced with nanotitania. *J. Electrochem. Soc.* **2016**, *163* (8), H664−H671.
(31) Li, R. L.; Lin, C.-W.; Shao, Y.; Chang, C. W.; Yao, F.-K.; Kowal, M. D.; Wang, H.; Yeung, M. T.; Huang, S.-C.; Kaner, R. B. Characterization of aniline tetramer by MALDI TOF mass spectrometry upon oxidative and reductive cycling. *Polymers* **2016**, *8*, No. 410.
(32) Narula, P.; Varinder, K.; Raghubir, S.; Sushil, K. K. Development of molecularly imprinted microspheres for the fast uptake of 4-cumylphenol from water and soil samples. *J. Sep. Sci.* **2014**, *37*, 3330−3338.
(33) Wong, Y. C.; Szeto, Y. S.; Cheung, W. H.; McKay, G. Pseudo-first-order kinetic studies of the sorption of acid dyes onto chitosan. *J. Appl. Polym. Sci.* **2004**, *92*, 1633−1645.
(34) Ho, Y. S.; McKay, G. Pseudo-second order model for sorption processes. *Process Biochem.* **1999**, *34*, 451−465.
(35) Yuh-Shan, H. Citation review of Lagergren kinetic rate equation on adsorption reactions. *Scientometrics* **2004**, *59*, 171−177.
(36) Kumar, K. V. Pseudo-second order models for the adsorption of safranin onto activated carbon: Comparison of linear and non-linear regression methods. *J. Hazard. Mater.* **2007**, *142*, 564−567.
(37) Majumdar, S.; Saikia, U.; Mahanta, D. Polyaniline-coated filter papers: Cost effective hybrid materials for adsorption of dyes. *J. Chem. Eng. Data* **2015**, *60* (11), 3382−3391.
(38) Langmuir, I. The adsorption of gases on plane surfaces of glass, mica and platinum. *J. Am. Chem. Soc.* **1918**, *40* (9), 1361−1403.
(39) Volmer, M. Thermodynamische Folgerungen ans der Zustandsgleichung für adsorbierte Stoffe. *Z. Phys. Chem.* **1925**, *115U* (1), 253−260.
(40) Faby, J.-A. L'utilisation des eaux usées épurées en irrigation, Document Technique FNDAE 1998, 11.
(41) Khader, E. H.; Mohammed, T. J.; Albayati, T. M. Comparative performance between rice husk and granular activated carbon for the removal of azo tartrazine dye from aqueous solution. *Desalin. Water Treat.* **2021**, *229*, 372−383.
(42) Shokry, H.; Elkady, M.; Hamad, H. Nano activated carbon from industrial mine coal as adsorbents for removal of dye from simulated textile wastewater: Operational parameters and mechanism study. *J. Mater. Res. Technol.* **2019**, *8*, 4477−4488.
(43) Pathania, D.; Sharma, S.; Singh, P. Removal of methylene blue by adsorption onto activated carbon developed from *Ficus carica* bast. *Arabian J. Chem.* **2017**, *10*, S1445−S1451.
(44) Sulyman, M.; Gierak, A. Green environmental approach for adsorption of hazardous dye from water using tree and sea plant leaves (dead L.). *Acta Sci. Agric.* **2020**, *4*, 1−10.
(45) Değermenci, G. D.; Değermenci, N.; Ayvaoğlu, V.; Durmaz, E.; Çakır, D.; Akan, E. Adsorption of reactive dyes on lignocellulosic waste; characterization, equilibrium, kinetic and thermodynamic studies. *J. Cleaner Prod.* **2019**, *225*, 1220−1229.
(46) Dawood, S.; Sen, T. K.; Phan, C. Synthesis and characterization of slow pyrolysis pinecone biochar in the removal of organic and inorganic pollutants from aqueous solution by adsorption: Kinetic, equilibrium, mechanism and thermodynamic. *Bioresour. Technol.* **2017**, *246*, 76−81.
(47) Malik, A.; Khan, A.; Anwar, N.; Muhammad, N. A comparative study of the adsorption of congo red dye on rice husk, rice husk char and chemically modified rice husk char from aqueous media. *Bull. Chem. Soc. Ethiop.* **2020**, *34*, 41−54.
(48) Praipipat, P.; Ngamsurach, P.; Saekrathok, C.; Phomtai, S. Chicken and duck eggshell beads modified with iron (III) oxide-hydroxide and zinc oxide for reactive blue 4 dye removal. *Arabian J. Chem.* **2022**, *15*, No. 104291.

https://doi.org/10.1021/acsomega.3c09031
ACS Omega 2024, 9, 15935−15949

(49) Praipipat, P.; Ngamsurach, P.; Prasongdee, V. Comparative reactive blue 4 dye removal by lemon peel bead doping with iron(III) oxide-hydroxide and zinc oxide. *ACS Omega* **2022**, *7*, 41744−41758.
(50) Loulidi, I.; Boukhlifi, F.; Ouchabi, M.; Amar, A.; Jabri, M.; Kali, A.; Chraibi, S.; Hadey, C.; Aziz, F. Adsorption of crystal violet onto an agricultural waste residue: kinetics, isotherm, thermodynamics, and mechanism of adsorption. *Sci. World J.* **2020**, *2020*, No. 5873521.

https://doi.org/10.1021/acsomega.3c09031
ACS Omega 2024, 9, 15935−15949